REPORT DOCUMENTATION PAGE

PLEASE DO NOT RETURN YOUR FORM TO THE ABOVE ADDRESS.

1. REPORT DATE	2. REPORT TYPE	3. DATES COVERED
July 1, 2012	Quarterly	April 1, 2012 to May 31, 2012

4. TITLE AND SUBTITLE

Thin Film Photovoltaic Cells on Flexible Substrates Integrated with Energy Storage

5a. CONTRACT NUMBER

5b. GRANT NUMBER

N00014-11-1-0658

5c. PROGRAM ELEMENT NUMBER

6. AUTHOR(S)

Westgate, Charles R. Sr.
Director of the Center for Autonomous Solar Power

5d. PROJECT NUMBER

5e. TASK NUMBER

5f. WORK UNIT NUMBER

7. PERFORMING ORGANIZATION NAME(S) AND ADDRESS(ES)

Center for Autonomous Solar Power
Binghamton University
85 Murray Hill Road
Vestal, Ny 13850

8. PERFORMING ORGANIZATION REPORT NUMBER

Q-July-2012

9. SPONSORING/MONITORING AGENCY NAME(S) AND ADDRESS(ES)

Office of Naval Research
875 North Randolf Road
Arlington, VA 22203-1995

10. SPONSOR/MONITOR'S ACRONYM(S)

ONR

11. SPONSOR/MONITOR'S REPORT NUMBER(S)

12. DISTRIBUTION/AVAILABILITY STATEMENT

Unlimited, public

13. SUPPLEMENTARY NOTES

14. ABSTRACT

The goals of the research programs in the Center for Autonomous Solar Power are to conduct research and development in thin film solar cells on flexible substrates for low cost fabrication on roll-to-roll manufacturing. The materials chosen are earth abundant and non-toxic. The expected outcome is very low cost solar cells that will be competitive in performance and well below current market prices in dollars/watt. Flexible solar cells are useful in building integrated photovoltaic systems and in military applications in austere environments.

A related research program focuses on ultracapacitors using new materials. With sufficiently high energy densities, ultracapacitors can replace batteries for energy storage and offer other advantages in long lifetimes and in tolerating operating temperature ranges.

15. SUBJECT TERMS

16. SECURITY CLASSIFICATION OF:			17. LIMITATION OF ABSTRACT	18. NUMBER OF PAGES	19a. NAME OF RESPONSIBLE PERSON
a. REPORT	b. ABSTRACT	c. THIS PAGE			Charles R. Westgate
U	U	U	UU	14	19b. TELEPHONE NUMBER: 607-777-6598

Standard Form 298

20120730024

Center for Autonomous Solar Power

ONR Award N00014-11-1-0658

PI: Charles R. Westgate
Binghamton University
Binghamton, NY 13902
607-777-6598
607-777-5780 (fax)
westgate@binghamton.edu

Reporting Period: April 1 through June 30, 2012
Date: July 20, 2012

Project Overview:

The major goals of the center are to develop and demonstrate new low cost solar cells that utilize earth-abundant and safe materials, For wide spread application of solar cells, it is necessary to reduce the costs substantially, thus the center will focus on fabrication of solar cells that are light weight and flexible. The roll-to-roll technology available at Binghamton University in the Center for Advanced Microelectronics Manufacturing (CAMM) offers unique opportunities to achieve these goals.

Another major goal is to work with industry and other partners to development new technologies for defense, energy, consumer, and industrial products related to solar power sources. The center will thus foster economic development through innovation and technology transfer to benefit our region and the nation.

TASK Report

Current research projects in the center include:

- Transparent conductors for solar cells
- Thin film solar cells using earth abundant materials with three candidate p-type absorbers
- Ultracapacitors for solar energy systems
- Reliability and durability of thin film solar devices
- Thermoelectric solar devices
- Hybrid organic/inorganic solar cells

Five of these topics will be discussed below. Results of the organic/inorganic solar cells will be included in the next report.

1. Summary of activities in the last quarter

Much of the emphasis in this quarter has been placed on fabrication and testing of solar cells using the p-type substrates zinc phosphide, iron disulfide, and CZTS. The n-type layers used are either zinc sulfide or cadmium sulfide, and the transparent conductor is aluminum doped zinc oxide. It is difficult to make efficient solar cells with larger areas in a non-clean room environment, thus cell areas are 1 cm^2 or less. New analytical analysis using photoluminescence and quantum efficiency were employed to characterize the cells. Relatively low efficiencies were observed and attributed to defects in the cells and individual layers or to deposition processes of the p-type substrate. {Note added: for CZTS, efficiencies of approximately 5% were observed for the sputtering method. Full report in the annual report for 2012.} We are confident about the n-type layers, transparent conductor, and measurement methods..

A replacement Atomic Layer Deposition (ALD) instrument has been delivered. The previous instrument was on loan and recalled by the University of Puerto Rico. This instrument is critical for the thin zinc oxide buffer layer between the transparent conductor and the transparent conductor, aluminum doped zinc oxide. The layers formed by the ALD are uniform and conformal, and will improve our cell performance.

Several methods for depositing CZTS are underway. The most successful method uses hydrazine, a highly toxic and unstable chemical, one that we cannot use in our laboratory. Our best layers are formed by pulsed laser deposition; however, a variety of other methods are investigation and testing that are appropriate for roll-to-roll fabrication. Three of the alternative methods are described below. Pulsed laser deposition has been discussed in earlier reports, and additional information will be provided in a later report.

Good progress has been made on thermoelectric materials with high figure of merits, Z_T. An interim report follows. In reliability, CASP is now testing Willow Glass from Corning, a flexible glass product suitable for solar cells. This product has been tested on the roll-to-roll facilities at Binghamton, and we have coated the glass with a transparent conductor under bending conditions commonly encountered in manufacturing and use.

In ultracapacitor research, experiments are underway with grapheme, and a report follows below. Results shows higher energy density storage is possible, and grapheme work will continue in the next quarter. A local manufacturer of ultracapacitors has agreed to provide independent testing of our capacitors using standard, industrial methods.

2. Effect of precursor sequence for CZTS thin films using elemental targets

Parag Vasekar, Research Scientist

In CZTS thin films, it is very important to maintain the Cu/(Zn+Sn) ratio around 0.9 and Zn/Sn > 1.0 in order to get device-quality, while yield good morphology and grain size in the films. It has been observed earlier that the precursor sequence affects the device quality. In recent experiments, four different combinations of precursor sequence were studied: 1. Cu/Sn/Zn 2. Sn/Cu/Zn 3. Sn/Zn/Cu and 4. Zn/Sn/Cu, where the first metal in sequence is deposited first and other two follow the deposition sequence. Tin being a low melting point metal has been avoided to be the last in all sequences. So far the best results are obtained for Sn/Cu/Zn sequence. As shown in Fig.1, the grains are very compact in 1.5-2 microns range and the absorber thickness is around 1 micron. Devices will be completed with the films synthesized using this sequence in the near future.

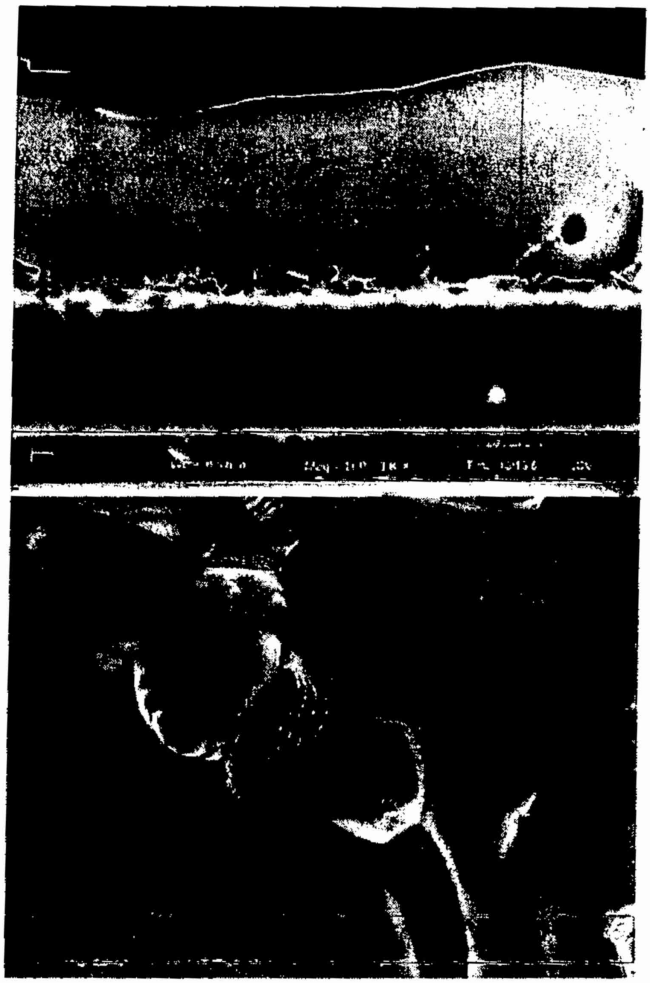

Fig.1. Cross-section and surface view of the CZTS film synthesized using Sn/Cu/Zn precursor deposition sequence.

1. Synthesis of Tin Sulfide using a Two Stage Process

Parag Vasekar, Research Scientist

Tin sulfide has been observed to be one of binary phases that forms as a secondary by-product during the synthesis of CZTS solar cells. Study of the growth kinetics of secondary phases is essential in order to understand the growth process of CZTS. We have started some experiments on the formation of tin sulfide to understand its growth process and because tin sulfide (SnS) is also a metal chalcogenide semiconductor material from the IV-VI group, it happens to be another alternative for an earth-abundant absorber. It has a near optimum direct bandgap of 1.35 eV and also a very good absorption co-efficient (10^5 cm^{-1}). Elements tin and sulfur and abundantly available. We have started synthesis of SnS using a two-stage process : sputtering of Sn metal followed by sulfurization. For sulfurization three different sources of sulfur and three different processes are used. The sulfur sources are H_2S, di-tert butyl disulfide and elemental sulfur

powder and the respective processes are conventional furnace annealing, chemical vapor deposition and rapid thermal processing. We intend to study the comparative growth processes in all three versions. It is observed that the optimum temperature range for tin sulfide formation is common for all three sulfurization routes and is around 325-350°C. Initial results are quite encouraging.

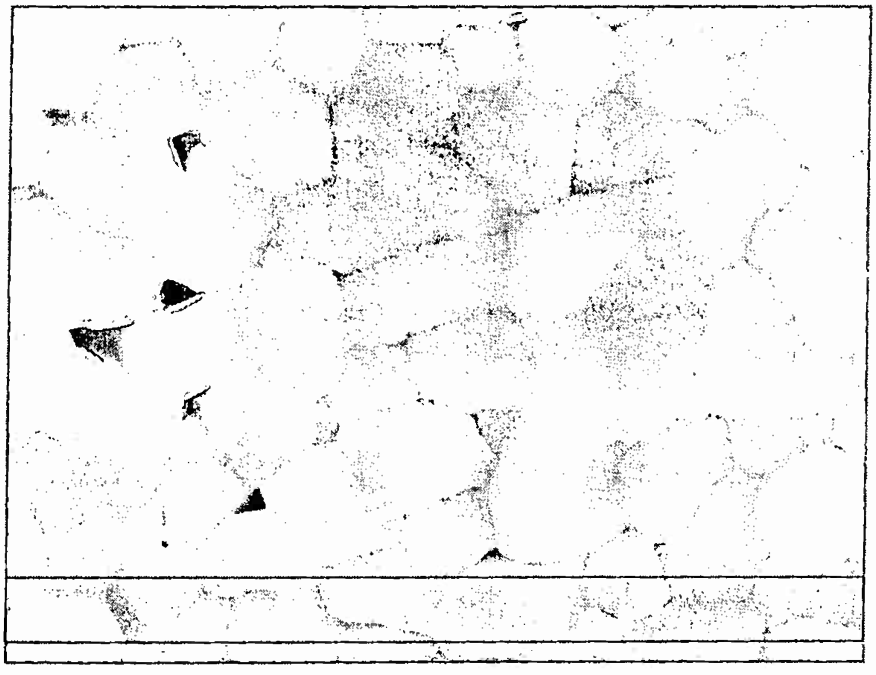

Fig 2. Tin sulfide film formed at 350°C using H_2S.

2. Growth of Cu_2ZnSS_4 (CZTS) by Sputtering

Tara Dhakal, Research Scientist

In the earlier reports, we had given a preliminary data on the growth of CZTS grown by sputtering process using a stoichiometric target. We encountered difficulties transferring the target material stoichiometrically into the substrate. Thus we began a growth study of CZTS thin film with three different targets, copper (Cu), tin sulphide (SnS) and zinc sulphide (ZnS). This allowed us to growth of CZTS with controlled ratios of Cu/Zn+Sn and Zn/Sn, which are important for optimal photovoltaic performance. The following figure shows the composition of the elements of CZTS with varying powers applied to Cu, SnS and ZnS targets.

Growth optimization:

The Cu target was subjected to DC power supply of 45W to 50W. RF power was used for the SnS and ZnS targets. For SnS, the powers were varied between 75 and 80 watts. For ZnS, 200W was used because this was the power to most efficiently sputter this material. The compositions shown were corrected using standards of Cu, Zn, Sn and S crystals. In can be seen from the graph below that we have good control and have to ability to change the composition of the various elements. As an example, the green curve in figure 1 shows the decrease of Cu

composition when the power decreased from 50W (for 040412a and 040412b) to 45 W (for 040412c and 040412d). Similarly, looking at the red curve it is clear that the amount of Sn in the sample decreased when the powers were decreased from 80W (for 040412a and 040412c) to 75W (for 040412b and 040412d).

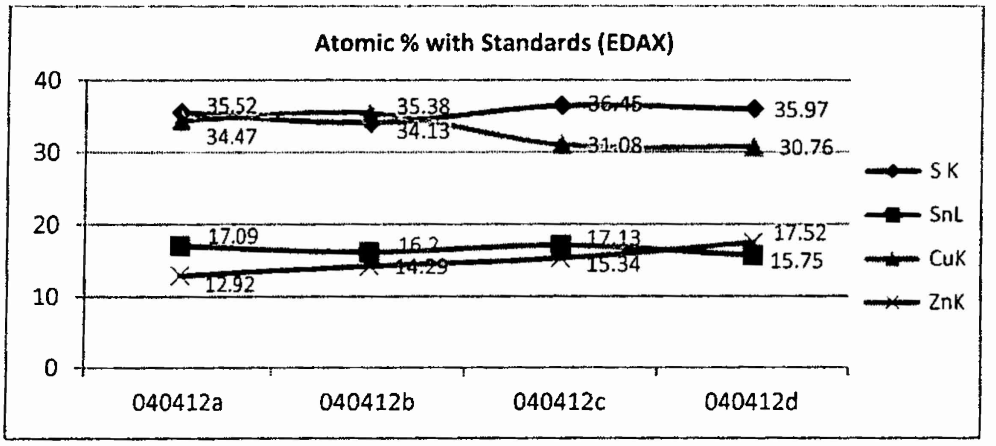

Figure 1. Composition of various samples of CZTS thin films grown on glass substrates.

The ratios of Cu/Zn+Sn and Zn/Sn are important for CZTS cell performance. The effort is to make copper poor and zinc rich samples. As can be seen in Table ,1 the ratios of Cu/Zn+Sn and Zn/Sn in the optimal sample (040412d) in this case are 0.92 and 1.11 respectively. The sample becomes consistently copper poor and zinc rich as we go from 040412a to 040412d. The powers used for Cu, SnS and ZnS used for the optimal sample (040412d) were 45W, 75W and 200W respectively. We have prepared this sample for cell fabrication.

Table 1. Elemental compositions and ratios of various elements in the CZTS film.

Elements/ratios	040412a (At. %)	040412b (At. %)	040412c (At. %)	040412d (At. %)
S K	35.52	34.13	36.45	35.97
SnL	17.09	16.20	17.13	15.75
CuK	34.47	35.38	31.08	30.76
ZnK	12.92	14.29	15.34	17.52
Cu/Zn+Sn	1.15	1.16	0.96	**0.92**
Zn/Sn	0.76	0.88	0.90	**1.11**

Annealing of the CZTS layer:

Although the samples had the right composition ratios, it was necessary to sulphurize the samples to get the kesterite phase for a right band gap. After the film was sulphurized in H_2S environment above 500°C shows a band gap of 1.44 eV (Fig. 2).

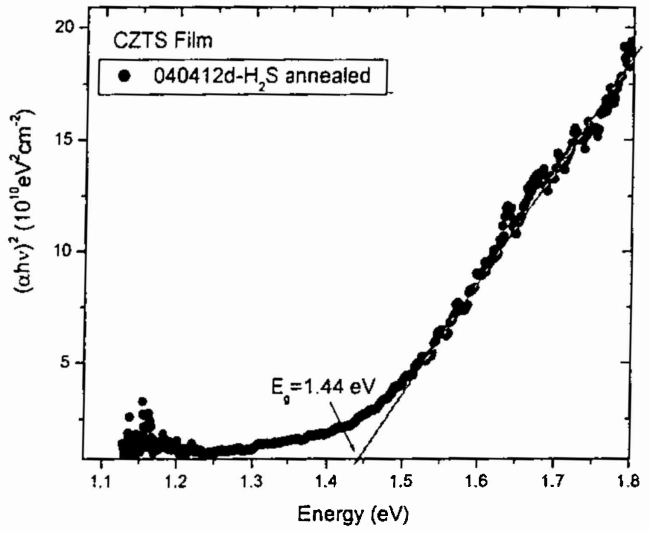

Figure 2. Band gap estimation of the sulphurized CZTS sample from the absorbance data.

Quantum Efficiency

Two cells were prepared for IV-testing from the sample 040412d. In one case the CZTS film was annealed in H_2S environment for 2 hrs. and in another case, it was annealed in H_2S for 2hrs and then annealed in N_2 for 2 hrs. before putting CdS and ZnO layers for cell fabrication. The quantum efficiencies of the two cells are shown in figure 3 below. It is clear that the sample annealed in additional 2 hrs. in nitrogen has higher quantum efficiency. For only H_2S annealed sample, the quantum efficiency is very low for higher wavelengths and increases very sharply at the wavelength near the band gap energy of zinc oxide and CdS. The triangular nature of the EQE is due to the low density of uncompensated acceptor concentrations. But after annealing in nitrogen subsequent to H_2S annealing improved the quantum efficiency (red curve in Fig. 3). The initial increase in EQE is due to the efficient photo-generated carriers from the bulk of the film caused by the expansion of the depletion layer. But the widening of the depletion layer weakens the electric field creating a favorable condition for surface recombination. Thus we see a significant decay in the EQE at lower wavelengths caused by surface recombination and the quantum efficiency decreases. However, as the density of acceptor concentrations increased by N_2 annealing, the surface recombination was reduced and the quantum efficiency was enhanced in the range of wavelengths between 350 nm to around 850 nm.

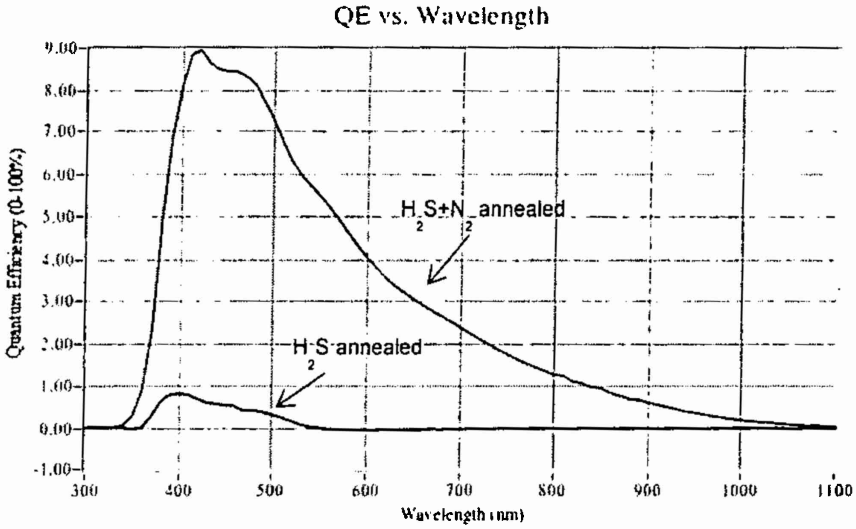

Future plans:

Photo-carrier generation in thin film solar cell is limited by the minority carrier diffusion through the absorber layer. Voltage bias on the device and its dependence on quantum efficiency are important to analyze effect of the defects on the minority carrier transport across the absorber layer. Our next focus will be to optimize the nitrogen annealing to improve the acceptor density and minimizing the defects in the layers to **Hi ZT Silicon Quarterly Progress:**

In this program, the development of sustainable, silicon based thermoelectric materials with large figure of merit (>3) is underway. Previously, it has been shown through molecular dynamics simulations that the thermal conductivity of Si containing random monolayers of Sn can be reduced by factors up to 3000 (i.e. to values of approximately 0.050 W/m-K) when 20% of the Si [100] planes are randomly selected and replaced with Sn. The random, mass altered atomic planes produce Anderson localization of the lattice vibrations which results in a dramatically reduced lattice thermal conductivity. Under conditions in which the mass-altered planes are the predominant source of charge carrier scattering, the expected ZT of such a solid for heat/transport in the cross-plane direction is expected to be greater than 8.

3. **High ZT Silicon (Thermoelectric)**

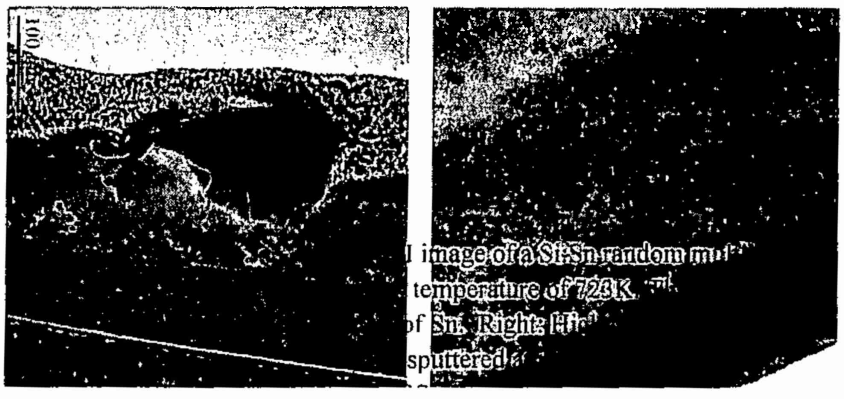

Bruce White, Associate Professor of Physics

During the last quarter, transmission electron microscopy, x-ray diffraction, atomic force microscopy, x-ray

photoemission spectroscopy, optical absorption, and cross-polarized optical microscopy have been carried out to physical examine the structures. Transmission electron microscopy revealed that samples prepared at substrate temperatures of 723K (Figure 1 left), result in non-planar thin films with significant agglomeration of Sn. However, when the substrate temperature is kept near room temperature (Figure 1 right), planar films are deposited with no evidence of Sn agglomeration.

X-ray diffraction results from the thin films deposited at 723K (figure 2) indicate the presence of both crystalline Si and Sn, confirming the Sn agglomeration results from TEM. Diffraction results from the room temperature deposited random multilayer thin film indicate only a broad amorphous peak, as expected, with no indication of agglomerated Sn. Rapid thermal annealing is being explored as a means to crystallize the room temperature deposited random multilayers, with promising initial results that will be reported next quarter.

Optical absorption studies of the room temperature deposited random multilayer indicate a bandgap consistent with that expected for a-Si while hall measurements indicate a low carrier concentration, below $10^{18}/cm^3$. Thus, the presence of the Sn planes does not appear to be causing significant increases in the carrier concentration. This is critical to maintaining a larger Seebeck coefficient in this material.

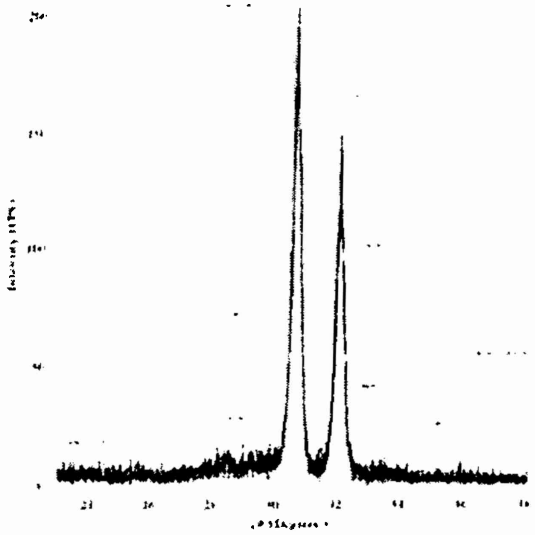

Figure 2 $\theta - 2\theta$ x-ray diffraction scans a Si:Sn random multilayer thin film deposited at 723K. Diffraction peaks from Si and Sn are observed, indicating that some agglomeration of Sn is taking place during sample generation.

Random Multilayer Variability:

To examine the variability that can exist in the number of low thermal conductivity modes (i.e. Anderson localized modes) in a Si:Sn system in which the percentage of randomly selected mass-altered planes is varied, we have constructed a simple one-dimensional lattice that approximates the solids simulated previously with molecular dynamics. In this model a single atom represents a plane of atoms in a bulk solid. The forces between atoms are modeled as ideal harmonic springs with a spring constant chosen to produce the correct longitudinal speed of sound in silicon. As in the case of the molecular dynamics simulations, we randomly select a number of atoms (representing planes) to be mass altered. In this case, we examine the Si:Sn system so that the mass ratio of the heavy atoms is approximately 4. The results of this work are shown in figure 3. The horizontal axis in figure 3 is

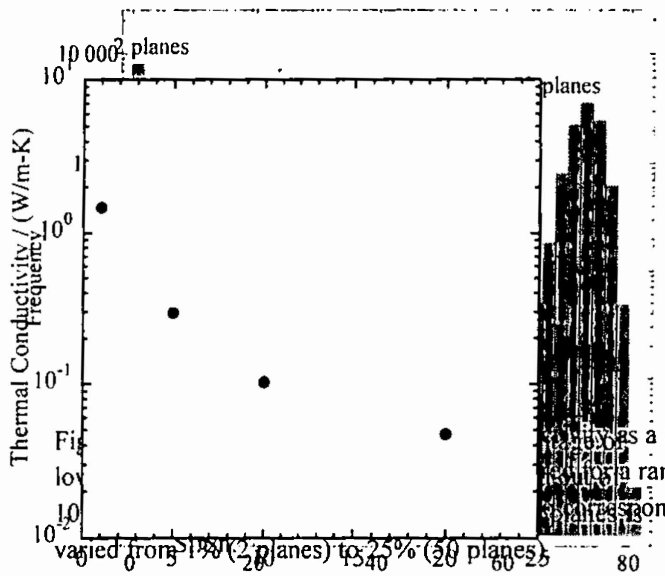

Fig... as a function o... from a random ...sponding to varied from 1% (2 planes) to 25% (50 planes).

the percentage of modes with inverse participation ration, R, greater than 0.05. Examination of the eigenmodes of vibration for this lattice indicate that for inverse participation ratios greater than 0.05, the eigenmode is localized and thus has zero thermal conductivity (ideally). The vertical axis of figure 3 is the number of times a given inverse participation ratio,occurs when random atoms are chosen to be mass altered. The random selection of atoms is performed 10000 times for each number of planes indicated in the figure (2 planes (1% mass altered planes), 5 planes (2.5 percent mass altered planes), 10 planes (5 percent mass altered planes), 20 planes (10% mass altered planes), and 50 planes (25% mass altered planes). As expected, as the number of mass altered planes increases, the distribution of the number of low thermal conductivity modes becomes tighter. For example, in the case in which 50 planes are mass altered, the percentage of modes with low lattice thermal conductivity varies from approximately 60% up to 80%. When only 20 planes are mass altered, this same percentage now varies from approximately 16% to 70%. Thus mass altering a larger number of planes minimizes variations that can occur in the properties of these random multilayers. In addition, this simulation allows us to determine the "ideal" random multilayer configuration that produced the largest number of localized, low thermal conductivity modes.

We examined the thermal conductivity of a Si:Sn system in which the percentage of atomic planes occupied by Sn atoms is varied from 1% to 20% (see figure 1) and the thermal conductivity is determined using reverse nonequilibrium molecular dynamics techniques . The simulations were carried out using the National Institute of Computational Science 112000 core Cray XT5 supercomputer at Oak Ridge National Laboratory. The results of the simulations are shown in figure 4. The results indicate that the thermal conductivity of this random multilayer system increases rapidly as the percentage of mass altered planes is reduced from 20% to 1% but approaches an asymptotic limit as the percentage of mass altered planes approaches 20%. While it is likely that small reductions in the thermal conductivity of this system can be achieved as the percentage of mass altered planes increases from 20% to 50%, this comes at the expense of increased process complexity. We note that as the concentration of mass altered planes increases above 50% we expect the thermal conductivity to rise as the thin film makes a transition from being a mixture of Si and Sn to being pure Sn.

Thus for our experimental work, we intend to continue our focus on utilizing 20% mass altered planes with mass ratios of 4.2 (corresponding to Sn atoms added to a silicon lattice).

Development of Solid State Supercapacitors Integrated with Solar cells for Solar Electricity Storage

This report embodies the research and development work carried out and the progress achieved in the major areas of the program of solid state supercapacitor for solar electricity storage. These areas and the major tasks therein are: (i) Supercapacitor Electrodes: We have investigated an approach to enhance the specific capacitance of conducting polymer poly(3,4-ethylenedioxythiophene) (PEDOT) by in situ incorporation of graphene to form composite film electrode. This is achieved by the synthesis of PEDOT films by an ultrashort galvanic pulsed electropolymerization technique in the presence of graphene. (ii) Solid-State Supercapacitors were fabricated using ionic liquid gel polymer electrolyte.

PEDOT/graphene composite electrode film synthesis

PEDOT-graphene composite films were electrochemically synthesized in a single step by a sequential galvanic pulse polymerization technique. The optimal conditions for making PEDOT-graphene films starts with the addition of 1 mg mL^{-1} of graphene powder in ethanol, which contained 0.1 M EDOT and 0.1 M $LiClO_4$ as dopant. The solution containing graphene powder and EDOT monomer was ultrasonicated at room temperature for 30 min to ensure proper dispersion of graphene. The pulsed electropolymerization was carried in a three electrode electrochemical cell over the flexible graphite sheet substrates, which was used as a working electrode. A platinum sheet was used as counter electrode and the electrochemical potentials were measured against a saturated Ag/AgCl reference electrode. The electropolymerization was carried out by applying sequential unipolar anodic current pulses of current density ~4 mA cm^{-2} for a very short period of time. Typically the anodic pulses were ON for 10 ms and the pulse OFF time was chosen as 100 ms. Total number of on pulses were set to complete a growth time equivalent of 200 s. For comparison, PEDOT films were also pulse electrodeposited onto flexible graphite sheet using similar solution without graphene

Preparation of ionic liquid based gel polymer electrolyte and Fabrication of supercapacitor cells

The ionic liquid gel electrolyte was prepared by a solution cast method. The host polymer poly(vinylidenefluoride-co-hexafluoropropylene) P(VdF-co-HFP) was separately dissolved in acetone. The ionic liquid 1-butyl-3- methylimidazolium tetrafluoroborate ($BMImBF_4$) was then mixed with the polymer solution and stirred magnetically for 10 h. The weight ratio of the ionic liquid $BMImBF_4$ to P(VdF-co-HFP) was kept at 4:1. The viscous solution of ionic liquid gel polymer electrolyte was used to fabricate solid-state supercapacitor cells.

PEDOT and PEDOT-graphene composite electrode based symmetrical solid-state supercapacitor cells were fabricated using ionic liquid gel polymer electrolyte in the following cell configurations:

Cell-I: PEDOT | gel polymer electrolyte | PEDOT
Cell-II: PEDOT-graphene | gel polymer electrolyte | PEDOT-graphene

Morphology of PEDOT-graphene composite electrodes

FE-SEM micrographs of the pulsed electropolymerized PEDOT and PEDOT-graphene composite films are shown in Figure 1. The microstructure of the PEDOT film comprises of irregularly shaped polymeric clusters of ~1-5 μm size. A close examination reveals, these cluster form with several small polymeric bundles thus producing high porous and rough surface texture as evident from the SEM micrograph in Fig. 1(a). The PEDOT-graphene film shows a heterogeneous composite microstructure resulting from significant changes in the polymerization by incorporation of graphene during the film growth as evidenced from the SEM micrograph shown in Fig. 1(b). The microstructure shows two different attributes region 1 and 2. The magnified image of region 1 is result of PEDOT polymer formation wrapped over graphene sheets (Fig. 1c). The region 2 is the graphene nanoplatelets embedded alongside or with the polymer clusters as shown in Fig. 1(d).

Fig. 1: FE-SEM images of (a) PEDOT film and (b) PEDOT-graphene composite film. The magnified image of region 1 and 2 of PEDOT-graphene film is shown in (c) and (d), respectively.

Performance studies on solid state supercapacitor cells

Fig. 2 shows the impedance spectra of both the symmetrical solid-state supercapacitor cells fabricated with ionic liquid gel polymer electrolyte. The steep rising behavior of the complex impedance plots in the low frequency region indicates the capacitive behavior, close to ideal capacitive characteristics, of both the supercapacitor cells with gel electrolytes. This technique enables the evaluation of various parameters associated with bulk properties of electrolytes and electrode- electrolyte interfaces including charge-transfer resistances, ion diffusion related resistance at the electrode-electrolyte interface, low frequency capacitance values, etc., to be evaluated separately in different frequency ranges. These resistances along with the capacitance values evaluated at frequency 10 mHz are listed in Table I. A comparison indicates that the supercapacitor Cell-II (with composite electrode) shows significant improved capacitance with substantial improved resistive parameter as compared to the Cell-I (with PEDOT electrode).

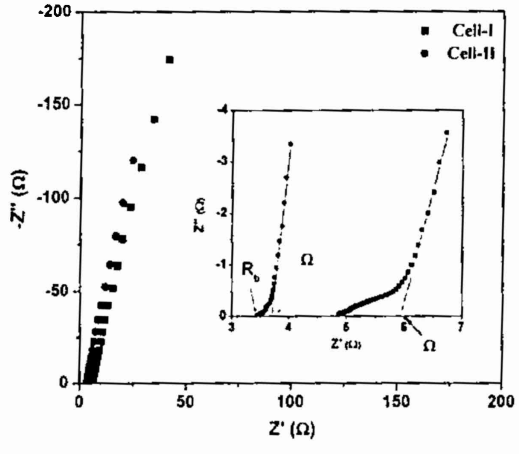

Fig. 2: Typical impedance plots of both the symmetrical supercapacitor cells (Cell-I & II with PEDOT and PEDOT-graphene composite electrodes, respectively) recorded at room temperature in the frequency ranging from 100 kHz to 10 mHz.

Table I. Electrical parameters of symmetrical supercapacitor cells from the impedance analysis

Supercapacitor cells	R_b (Ω cm^2)	Ω (Ω cm^2)	C^1 (mF cm^{-2})	C^2 (F g^{-1})
Cell-I	8.8	1.9	50.8	56

Cell-II	6.2	0.5	73.4	79.7

[1]Overall cell capacitance at 10 mHz; [2]Singel electrode capacitance at 10 mHz

The comparative performance of the solid-state supercapacitor cells (Cell-I & II) based on PEDOT and PEDOT-graphene composite electrodes were evaluated by cyclic voltammetry (CV) and galvanostatic charge-discharge tests. The PEDOT-graphene composite electrode shows better electroactivity compared to the PEDOT electrode as confirmed from these studies, shown in Fig. 3.

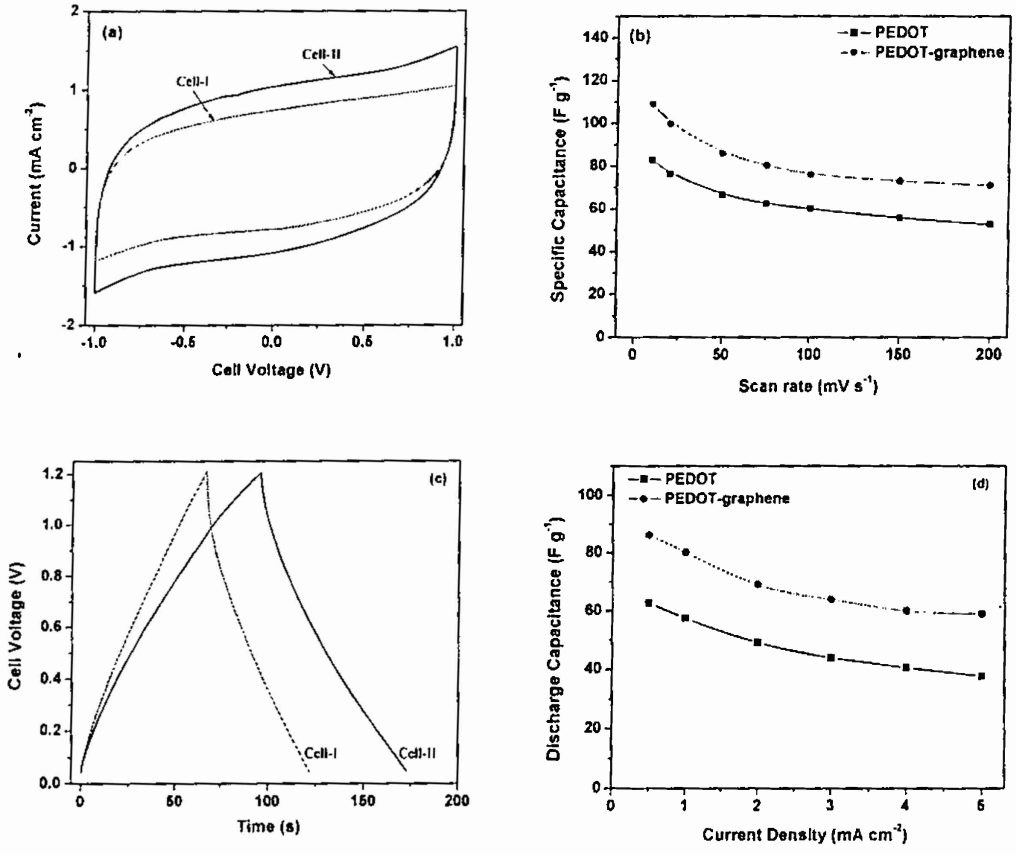

Fig. 3: (a) CV curves of both the supercapacitor cells (Cell-I & II) at scan rate 10 mV s^{-1} for direct comparison. (b) Variation in the specific capacitance of PEDOT and PEDOT-graphene composite electrodes, calculated from CV curves of both the supercapacitor cells, as a function of the scan rates. (c) Galvanostatic charge-discharge curves of the both the supercapacitor cells at current density of 1 mA cm^{-2}. (d) Variation in discharge capacitance (C_d) of both the electrodes, calculated from discharge curves of both the cells, as a function of current density.

Conclusion

The PEDOT-graphene composite performed better as supercapacitor electrode with enhanced capacitance of ~80 F g^{-1} as compared to the PEDOT electrodes (~56 F g^{-1}).

Publications submitted and/or accepted

1. Hamasha, M. M., Alazam, A. R., Hamasha, S. M., Aqlan, F., Almeanazel, O. T., Khasawneh, M. T., "Muti-Machine Flexible Manufacturing Cell Analysis Using Markov Chain Approach", (Submitted: International Journal of Advanced Manufacturing Technology).
2. Sudarsanam, H., Peng, C., Hamasha, M. M., Lu, S., and Westgate, C. R. "Cost effective green grid system (grid-tied photovoltaic system): a simulation-based optimization study", (Submitted: Journal of Management and Engineering Integration).
3. Peng, C., Hamasha, M. M., VanHart, D., Lu, S., Westgate, C. R.,"Electrical and optical degradation studies on aluminum-doped zinc oxide transparent conductive thin films under cyclic bending conditions" (Submitted: Thin Solid Films).
4. Hamasha, M. M., Dhakal, T., Vasekar, P., Alzoubi, K., Lu, S., Vanhart, D., Westgate, C. R., "Reliability of Sputtered Deposited Aluminum-Doped Zinc Oxide under Harsh Environmental Conditions", (Submitted: Solar Energy Materials & Solar Cells).
5. Hamasha, M. M., Alzoubi, K., Switzer III, J. C., Lu, S., Poliks, M., Westgate, C. R., "Reliability of Sputtered Aluminum Thin Film on Flexible Substrate under Cyclic Bending Fatigue Conditions", (Accepted: IEEE Transaction on Components, Packaging and Manufacturing Technology).
6. Parag Vasekar, Tara Dhakal, Laxmikanth Ganta, Daniel Vanhart and Seshu Desu, "Synthesis of Zinc Sulfide by CVD using a novel organometallic precursor: di-tertiary-butyl-disulfide", submitted to Thin Solid Films on November 18, 2011
7. Parag Vasekar, Siva P Adusumulli, Daniel Vanhart and Seshu Desu " Synthesis and growth mechanisms of zinc phosphide nanowires and thin film", submitted to Journal of Materials Science and Technology on May 10, 2012.
8. Parag Vasekar, Siva P Adusumulli, Daniel Vanhart, Tara Dhakal and Seshu Desu, " Development of zinc phosphide as a p-type absorber ", submitted on 38th photovoltaic specialists conference proceedings, Austin on May 21, 2012.
9. Parag Vasekar,Lakshmikanth Ganta, Surya Rajendran, Daniel Vanhart and Charles R. Westgate, "Growth and Characterization of CZTS films using TBDS as a sulfur source"", submitted to Solar Energy on April 4, 2012
10. Siva Pramod Adusumulli, Parag Vasekar, Daniel Vanhart and Tara Dhakal, "Synthesis of zinc phosphide thin film solar cells", submitted to MRS conference proceedings, SanFrasisco, in April 2012.